ACS Catalysis

Research Article

Cite This: ACS Catal. 2019, 9, 6766–6782

pubs.acs.org/acscatalysis

Redox Cofactor Rotates during Its Stepwise Decarboxylation: Molecular Mechanism of Conversion of Coproheme to Heme *b*

Lisa Milazzo,[†] Thomas Gabler,[‡] Dominic Pühringer,[§] Zuzana Jandova,[∥] Daniel Maresch,[‡] Hanna Michlits,[‡] Vera Pfanzagl,[‡] Kristina Djinović-Carugo,[§,⊥] Chris Oostenbrink,[∥] Paul G. Furtmüller,[‡] Christian Obinger,[‡] Giulietta Smulevich,*[,†] and Stefan Hofbauer*[,‡]

[†]Dipartimento di Chimica "Ugo Schiff", Università di Firenze, Via della Lastruccia 3-13, I-50019 Sesto Fiorentino (FI), Italy

[‡]Department of Chemistry, Division of Biochemistry, BOKU−University of Natural Resources and Life Sciences, Muthgasse 18, A-1190 Vienna, Austria

[§]Department for Structural and Computational Biology, Max F. Perutz Laboratories, University of Vienna, A-1030 Vienna, Austria

[∥]Department of Material Sciences and Process Engineering, Institute of Molecular Modeling and Simulation, BOKU−University of Natural Resources and Life Sciences, A-1190 Vienna, Austria

[⊥]Department of Biochemistry, Faculty of Chemistry and Chemical Technology, University of Ljubljana, 1000 Ljubljana, Slovenia

Supporting Information

ABSTRACT: Coproheme decarboxylase (ChdC) catalyzes the last step in the heme biosynthesis pathway of monoderm bacteria with coproheme acting both as redox cofactor and substrate. Hydrogen peroxide mediates the stepwise decarboxylation of propionates 2 and 4 of coproheme. Here we present the crystal structures of coproheme-loaded ChdC from *Listeria monocytogenes* (LmChdC) and the three-propionate intermediate, for which the propionate at position 2 (p2) has been converted to a vinyl group and is rotated by 90° compared to the coproheme complex structure. Single, double, and triple mutants of LmChdC, in which H-bonding interactions to propionates 2, 4, 6, and 7 were eliminated, allowed us to obtain the assignment of the coproheme propionates by resonance Raman spectroscopy and to follow the H_2O_2-mediated conversion of coproheme to heme *b*. Substitution of H_2O_2 by chlorite allowed us to monitor compound I formation in the inactive Y147H variant which lacks the catalytically essential Y147. This residue was demonstrated to be oxidized during turnover by using the spin-trap 2-methyl-2-nitrosopropane. Based on these findings and the data derived from molecular dynamics simulations of cofactor structures in distinct poses, we propose a reaction mechanism for the stepwise decarboxylation of coproheme that includes a 90° rotation of the intermediate three-propionate redox cofactor.

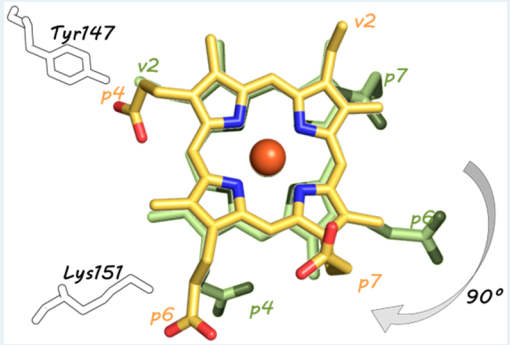

KEYWORDS: *heme biosynthesis, coproheme decarboxylase, Listeria monocytogenes, compound I, resonance Raman*

1. INTRODUCTION

Coproheme decarboxylase (ChdC, formerly known as HemQ) catalyzes the last step in the heme biosynthesis pathway of monoderm bacteria.[1] Two propionate groups from iron coproporphyrin III (coproheme) at positions 2 and 4 (p2, p4) are cleaved off to yield a three-propionate intermediate (monovinyl, monopropionate deuteroheme) and, finally, iron protoporphyrin IX (heme *b*).[2−4] The reaction is mediated by hydrogen peroxide and needs two H_2O_2 molecules to transform one coproheme to heme *b*.[5] Most interestingly, coproheme acts as both substrate and redox cofactor. ChdC loaded with nickel substituted coproheme is totally inactive and ChdC with manganese substituted coproheme is inactive toward H_2O_2 but can be oxidized by peroxyacetic acid.[2,6] Up to now biochemical studies were performed on ChdCs from Firmicutes, i.e. *Staphylococcus aureus* (SaChdC), *Listeria monocytogenes* (LmChdC), and *Geobacillus stearothermophilus* (GsChdC).[5,7−10]

Recently, DuBois and co-workers proposed a reaction mechanism of the decarboxylation reaction that involves a catalytic redox-active tyrosine residue (Y147, LmChdC numbering). This conserved aromatic residue was proposed to be oxidized by a (hypothetic) compound I [oxoiron(IV) Por$^{\bullet+}$] thereby producing compound I* [oxoiron(IV) $^{\bullet}$Y147], which initiates the decarboxylation reactions of p2 and p4.[6] Successively, transient formation of $^{\bullet}$Y147 was confirmed by electron paramagnetic resonance (EPR) spectroscopy.[11] While the proposed mechanism of the first propionyl decarboxylation (p2) is generally accepted (although experimental evidence for

Received: March 5, 2019
Revised: May 20, 2019
Published: June 18, 2019

DOI: 10.1021/acscatal.9b00963
ACS Catal. 2019, 9, 6766−6782

Table 1. Data Collection and Refinement Statistics

	coproheme/monovinyl, monopropionate deuteroheme-LmChdC (6FXQ)		coproheme-LmChdC (6FXJ)
	Data Collection		
wavelength (nm)	0.9537		1.0000
resolution range (Å)	47.08−1.69 (1.75−1.69)[a]		46.9−1.79 (1.85−1.79)[a]
space group	$P12_11$		$P12_11$
unit cell length *a*, *b*, *c* (Å)	77.69, 129.4, 77.92		77.87, 129.11, 77.92
unit cell angle α, β, γ (deg)	90, 105.52, 90		90, 105.9, 90
total reflections	471367 (46069)		475594 (47555)
unique reflections	162948 (16108)		134739 (13306)
multiplicity	2.9 (2.9)		3.5 (3.6)
completeness (%)	0.98 (0.98)		0.97 (0.96)
mean *I*/sigma (*I*)	2.93 (0.39)		6.98 (1.06)
Wilson B-factor (Å^2)	26.8		21.9
refinement	old (5LOQ)	new (6FXQ)	
R-merge (%)	18.9 (174.8)	18.9 (174.8)	13.4 (114.7)
R-meas (%)	23.1 (214.1)	23.1 (214.1)	15.9 (135.1)
R-pim (%)	13.1 (122.3)	13.1 (122.3)	8.3 (70.8)
CC1/2	0.96 (0.174)	0.96 (0.173)	0.99 (0.647)
CC*	0.99 (0.545)	0.99 (0.543)	0.99 (0.886)
reflections used in refinement	161813 (15055)	161810 (15055)	134661 (13294)
reflections used for R-free	1976 (185)	1976 (185)	2005 (196)
R-work (%)	18.4 (40.7)	17.8 (39.4)	16.8 (34.0)
R-free (%)	21.5 (41.9)	21.4 (39.4)	21.9 (37.5)
CC(work)	0.957 (0.511)	0.960 (0.513)	0.974 (0.842)
CC(free)	0.962 (0.643)	0.961 (0.637)	0.962 (0.733)
number of non-hydrogen atoms	10796	11024	11539
no. of atoms macromolecules	9801	9801	10060
no. of atoms ligands	282	512	293
no. of atoms solvent	713	711	1186
protein residues	1203	1203	1213
RMS (bonds) (Å)	0.011	0.014	0.011
RMS (angles) (deg)	1.12	1.2	1.04
Ramachandran favored (%)	99	98.6	98.7
Ramachandran allowed (%)	1.3	1.4	1.3
Ramachandran outliers (%)	0.084	0	0
rotamer outliers (%)	2.4	2.2	0.37
clashscore	1.68	1.86	2.72
average B-factor (Å^2)	38.5	39.3	33.2
macromolecules (Å^2)	37.5	38.3	31.9
ligands (Å^2)	68.4	54.7	46.9
solvent (Å^2)	41.5	42.1	41.2
number of TLS groups	50	50	1

[a]Values in parentheses are for the highest-resolution shell.

compound I formation is missing), the second decarboxylation reaction at the p4 position is still an open question. DuBois and co-workers proposed that decarboxylation of p4 may involve residues in the vicinity of p4, namely K151, W200, W159, and Y113 (LmChdC numbering). However, substitution of any of these residues did not result in complete loss of activity, the K151A mutant showed highly impaired reactivity toward p4 oxidation, and almost no formation of heme *b* was detected.[6,11] On the basis of these mutational studies and in support of Y147 involvement in the decarboxylation reactions of both p2 and p4, the possibility of a long (i.e., 10 Å) range proton-coupled electron transfer from p4 to Y147 was discussed with the three-propionate intermediate remaining in the same position as the coproheme substrate.[6] Since the catalytic tyrosine was shown to be essential for both decarboxylation reactions, a possible mechanism involving substrate reorientation has been suggested recently.[11]

The present work provides experimental evidence for the H_2O_2-mediated oxidation reaction of ferric LmChdC to compound I together with the rotation of the three-propionate intermediate by approximately 90° within the active site. This moves p4 to the former position of p2 and, thus, to be in close proximity of catalytic Y147 for initiation of the second decarboxylation cycle. Wild-type LmChdC and mutated proteins were studied by a broad range of biochemical and biophysical methods including X-ray crystallography, resonance Raman (RR) spectroscopy, mass spectrometry, UV−vis stopped-flow spectroscopy, and complemented by molecular dynamics (MD) simulations. We present (i) kinetic and spectroscopic evidence of coproheme compound I formation, (ii) identification of the Y147 radical by spin-trapping, (iii) the assignment of the bending modes [$\delta(C_\beta C_c C_d)$] of all four propionyl substituents of coproheme and the spectral transition to heme *b* mediated by H_2O_2, (iv) the crystal

DOI: 10.1021/acscatal.9b00963
ACS Catal. 2019, 9, 6766−6782

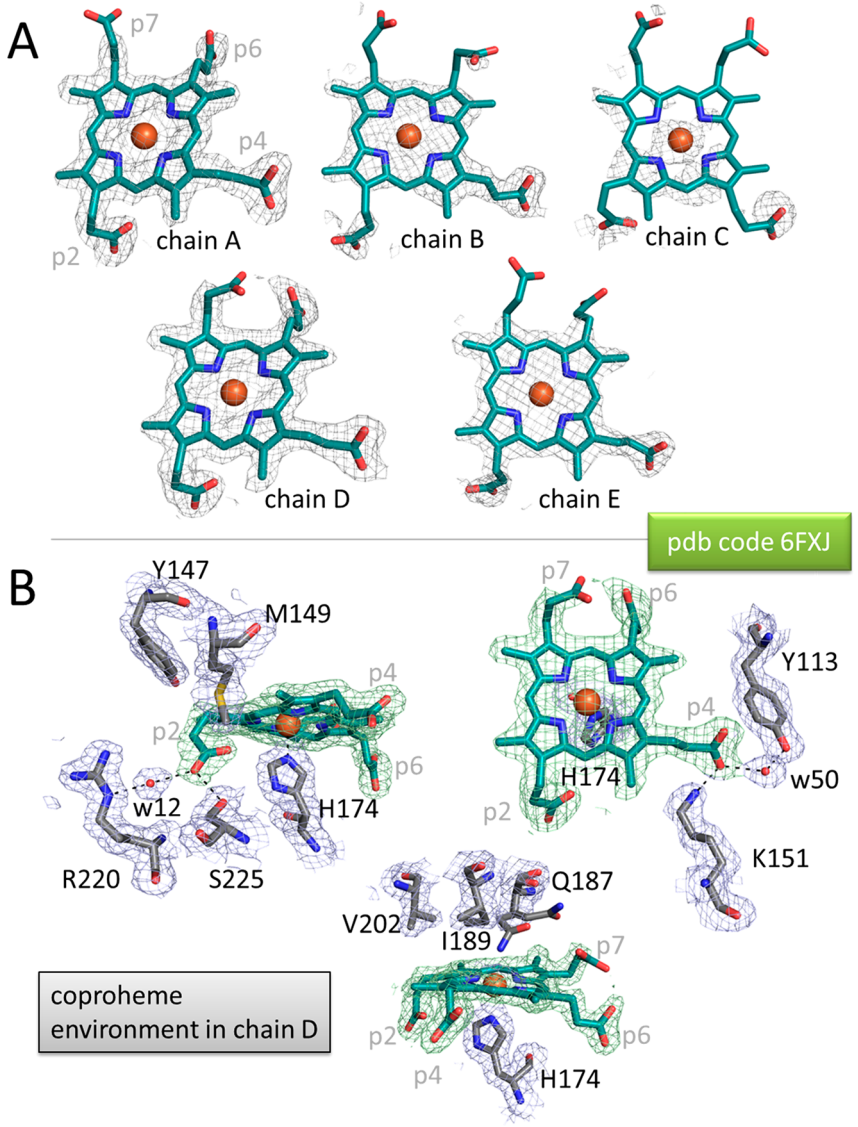

Figure 1. Active site structure of ferric coproheme-LmChdC (6FXJ). (A) Electron densities (σ = 1.0, gray mesh) and structural models (as green sticks) of coproheme bound to LmChdC in all five subunits. (B) Electron densities and structural model of the active site of coproheme-LmChdC (chain D) showing H-bonding interactions of p2 (left) and of p4 (right) as well as conserved residues in the coproheme cavity including the catalytic Y147, the flexible Q187, and the proximal coproheme ligand H174.

structures of coproheme-LmChdC and of monovinyl, monopropionate deuteroheme-LmChdC in the rotated orientation, and, finally, (v) we propose a mechanism for decarboxylation of coproheme and monovinyl, monopropionate deuteroheme.

2. RESULTS

2.1. Crystal Structures of Coproheme-LmChdC and Monovinyl, Monopropionate Deuteroheme-LmChdC in the Rotated Orientation. Coproheme decarboxylases have been shown to react with submicromolar H_2O_2, which initiates the decarboxylation of coproheme and thus provokes heterogeneity in the active site.[11] Consequently, the first crystal structure of coproheme-ChdC was obtained from catalytically inactive manganese-loaded coproheme-GsChdC.[6] Here, in order to obtain the crystal structure of iron-coproporphyrin III-loaded LmChdC, we inhibited residual enzymatic activity by addition of 5 mM cyanide to the crystallization drop. Cyanide was diluted out of the crystals prior to cryo-cooling with mother liquor. The crystals, grown in 0.1 M HEPES, pH 7.5, 20% (w/v) PEG 4000, 10% (v/v) 2-propanol, diffracted to a resolution of 1.79 Å (6FXJ). The protein crystallizes as a pentamer in space group $P12_11$ with unit cell parameters of 77.87 Å × 129.11 Å × 77.92 Å, almost identical to previously solved structures (Table 1).[5] The electron densities of coproheme allowed us to assign three out of four propionates (p2, p4, and p6) in chains A and D (Figure 1A). In general, the active site of coprohome-LmChdC very closely resembled that of Mn-coproheme-GsChdC in the resting state.[6] In chains A and D, the entire subunit could be modeled, since the flexible loop forming the active site access channel is stabilized by crystal packing contacts, similar to the previously solved structures of Firmicutes ChdCs (4WWS, 5LOQ, 5T2K).[5,6,9] Electron densities for coproheme in the other subunits (B, C, and E) were weak and do not allow to reliably refine the cofactor's coordinates (Figure 1A).

Analysis of the hydrogen bonding interactions of the four propionate groups in chains A and D reveals an extensive network spanning from p2 to p4 (R220−water−p2−S225−

DOI: 10.1021/acscatal.9b00963
ACS Catal. 2019, 9, 6766−6782

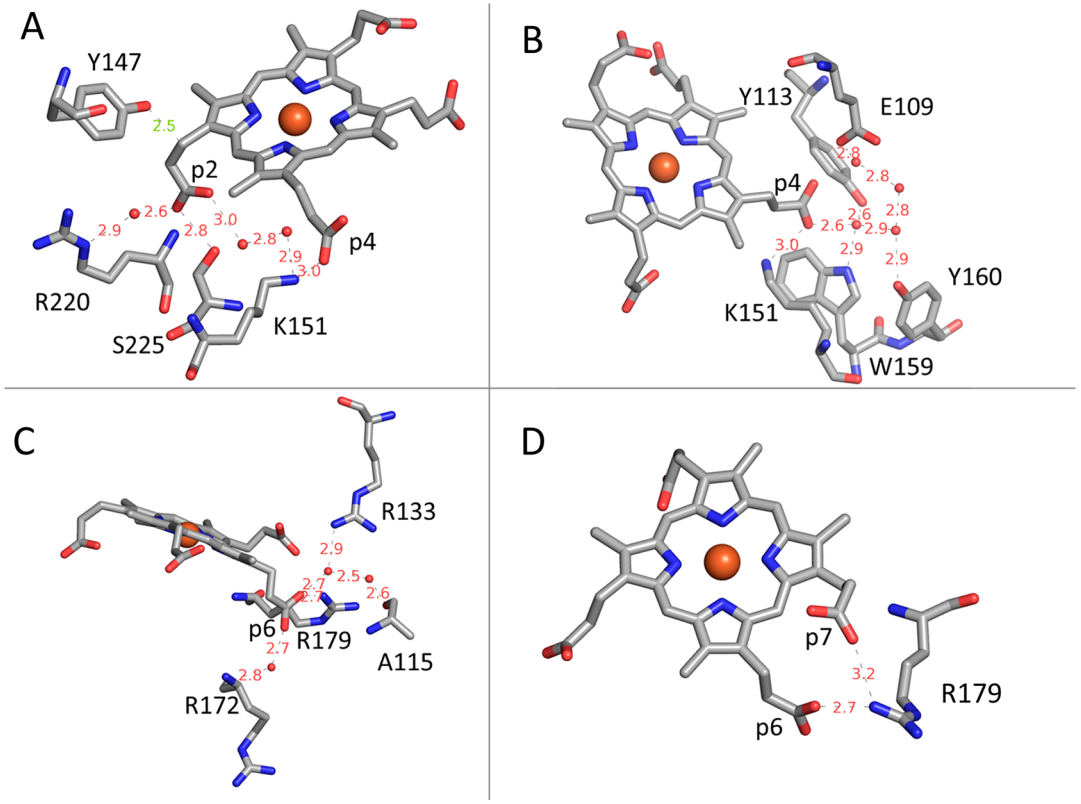

Figure 2. Hydrogen bonding interactions between oxygen atoms of propionates of coproheme and the protein moiety in the resting state (6FXJ, chain D). (A) H-bonding network around p2 and p4. The distance of catalytic Y147 to β-carbon of p2 is shown in green since it is the distance to a carbon atom; all other distances (to oxygen atoms) are shown in red. (B) Further H-bonding network of p4. (C, D) H-bond interactions of p6 and p7.

p2−water−water−K151−p4) (Figures 1B and 2). The propionate at position 6 (p6) is also stabilized and coordinated by various H-bonds (water, R172, R179, R133, and A115) in contrast to p7 (potentially H-bonded to R133 in chain D or Q187 in chain A), whose position is the most variable in all subunits. The hydrogen bonding interactions of p2, p4, p6, and p7 of all subunits are summarized in Table S1.

In the absence of cyanide during crystallization, LmChdC exhibits low activity even in the absence of exogenously added H_2O_2.[12] Apparently, submicromolar H_2O_2, which is always present in buffers under aerobic conditions, can initiate decarboxylation of coproheme. During initial studies we were not aware of this possible reaction, and in the previously reported crystal structure (in 0.1 M bicine pH 9.0, 10% w/v PEG 6000; 1.69 Å; pdb code 5LOQ) of the redox cofactor-loaded LmChdC,[5] we assigned p6 and p7 in analogy to heme *b* in chlorite dismutases, which share a similar fold.[13,14] By contrast, p2 and p4 could not be resolved. Presently, based on the structures of GsChdC complexed with manganese coproheme (5T2K)[6] and of coproheme-LmChdC (6FXJ) obtained by the approach described above, we revisited the data set of 5LOQ and built a new model with two porphyrin species having occupancies of 50% each (6FXQ). One species corresponds to iron coproporphyrin III in the orientation of the structure described above (6FXJ). The second species is an iron monovinyl, monopropionate deuteroheme rotated by 90° compared to the coproheme of the structures 5T2K and 6FXJ, and, therefore, in the orientation of the previously solved redox cofactor (5LOQ). With this new model the refinement statistics have been improved (Table 1).

In the new structural model (6FXQ) propionates p2 of coproheme and p4 of monovinyl, monopropionate deuteroheme share the same region in the active site and are H-bonded to S225 and R220 and close to the catalytic tyrosine (Y147), whereas p4 of coproheme and p6 of the three-propionate intermediate interact with K151 and Y113 (Figure 3). The densities (in chains A, D, and E) at position 2 of the monovinyl, monopropionate deuteroheme are clearly indicative of a vinyl group, rather than a methyl or even propionate group. This suggests that in the absence of cyanide (i) coproheme of LmChdC was partially converted to the three-propionate intermediate during crystal growth by oxygen activation and generation of hydrogen peroxide and (ii) that coproheme is present in a different orientation compared to the monovinyl, monopropionate deuteroheme. Both cofactors are 90° rotated with respect to each other, which is in agreement with the hypothesis that the cofactor rotates during decarboxylation and that both propionates are in close vicinity to the catalytic Y147 residue, which is involved in the decarboxylation reactions of both p2 and p4.

2.2. Dynamics of H-bonding in Coproheme-LmChdC and Monovinyl, Monopropionate Deuteroheme-LmChdC. In order to examine and compare the interactions of the two distinct binding poses of coproheme and the three propionates intermediate in LmChdC, we simulated both coproheme and monovinyl, monopropionyl deuteroheme with their p2/v2 and p4 propionates oriented toward catalytic Tyr147. The initial binding poses are summarized in Figure 4. Coproheme in pose 0 reflects the correct binding of the

DOI: 10.1021/acscatal.9b00963
ACS Catal. 2019, 9, 6766−6782

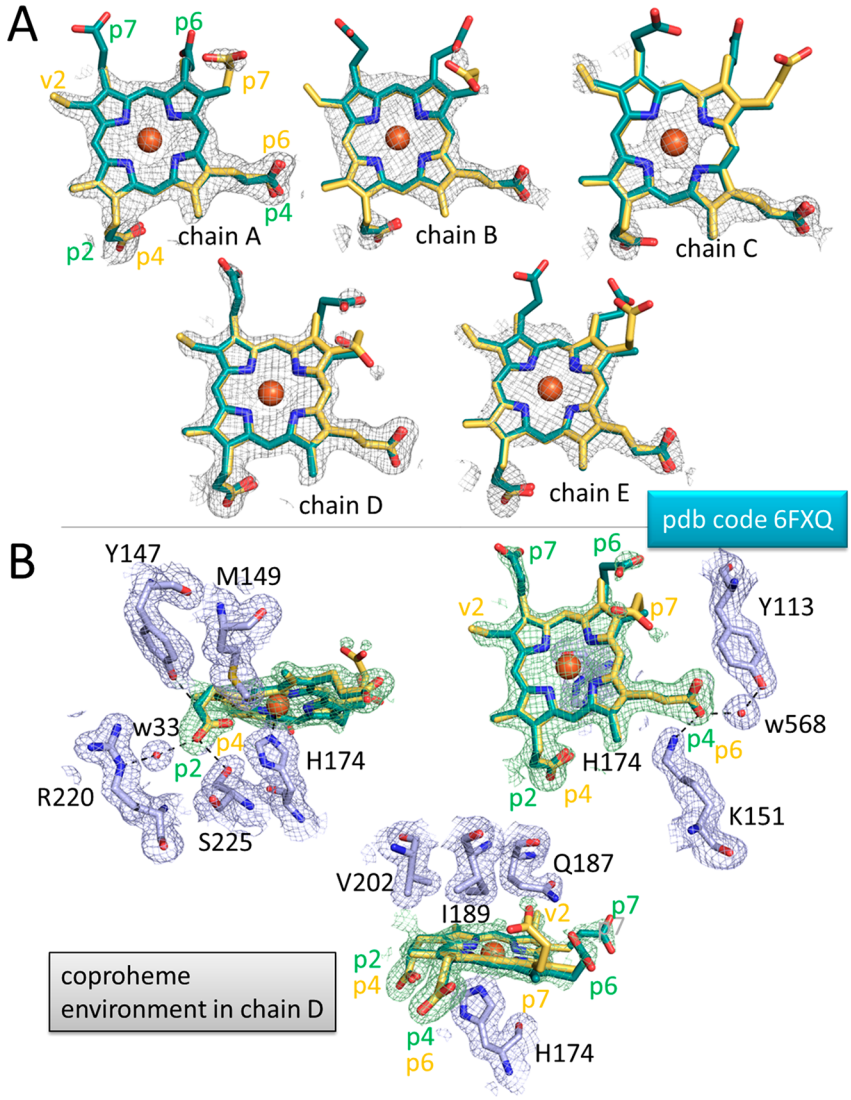

Figure 3. Active site structure of coproheme-LmChdC during turnover (6FXQ). The model is based on two cofactors with occupancies of 50% each, i.e. coproporphyrin III and rotated monovinyl, monopropionate deuteroheme. (A) Electron densities (σ = 1.0, gray mesh) and structural models of coproheme (green sticks) and monovinyl, monopropionate deuteroheme (yellow sticks) bound to LmChdC in all five subunits are depicted. (B) Electron densities and structural model of the active site of coproheme-LmChdC in chain D showing interactions of p2 (left) and p4 (right), as well as the distal and proximal sides of the redox cofactor (bottom).

substrate/redox cofactor in LmChdC (6FXJ) as reported in Figure 1.

Simulation of one pentamer comprises five redox cofactors bound to the five monomers, which provides good statistics, comparable to five separate monomer replicas. Table 2 summarizes the percentage of simulation time during which oxygens of propionates form H-bonds to amino acids of the active site. The highest hydrogen bonding frequency is observed between p2 and Tyr147 in coproheme in pose 0 (98% present during simulation). In this simulation p2 forms further H-bonds with Ser225 (95% of simulation time) and Phe231 (57%), thus being the strongest interacting propionate in all simulations (forming on average 2.5 hydrogen bonds). Coproheme in pose 90 shows the highest number of hydrogen bonds per cofactor with the highest contribution originating from p7 that interacts with Leu114, Ser116, and Ala115.

In the simulations of monovinyl, monopropionyl deuteroheme in pose 90 (i.e., rotated orientation), p4 forms more than two hydrogen bonds for 100% of the simulation time, including H-bonding with Tyr147 (74% of simulation time). On the other hand, in the simulations of monovinyl, monopropionyl deuteroheme in pose 0 a strong H-bond is established between p4 and Lys151 (94%). Overall, monovinyl, monopropionyl deuteroheme in pose 90 with p4 oriented toward Tyr147 forms more than twice as many H-bonds as coproheme in pose 0 with p2 being oriented toward Tyr147. This is a consequence of the strong hydrogen bonding interactions of p6 and p7 in the monovinyl, monopropionyl deuteroheme in pose 90.

Furthermore, we evaluated the probability of electron transfer to Tyr147 from the Cβ atom of propionates using Dijkstra's graph search algorithm (Table S2).[15−17] Figure 5 depicts the predicted electron transfer pathways. Since p2 is the first propionate to be cleaved off, there is a more than 118 times higher probability of electron transfer to Tyr147 if coproheme is in pose 0 compared to coproheme in pose 90. In the case of monovinyl, monopropionyl deuteroheme, the probability of electron transfer to Tyr147 from the Cβ atom of

DOI: 10.1021/acscatal.9b00963
ACS Catal. 2019, 9, 6766−6782

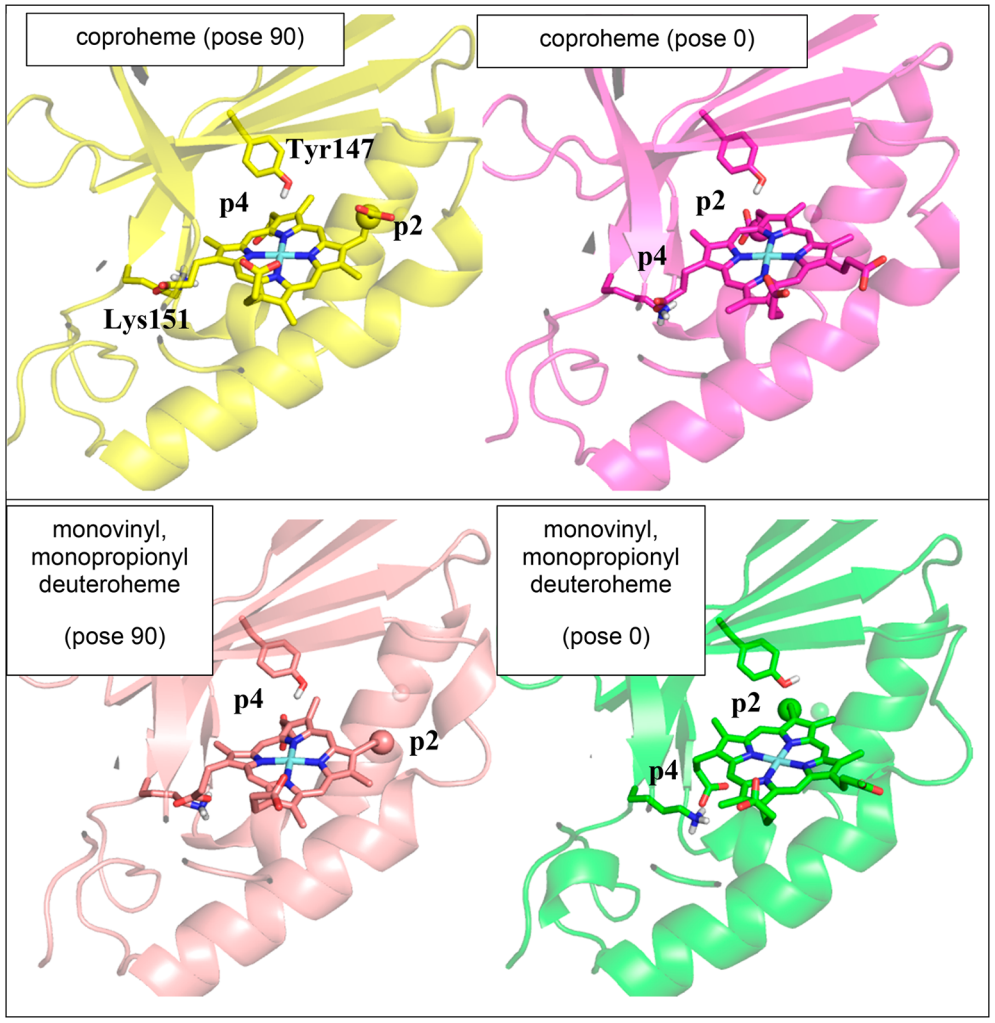

Figure 4. Snapshots of the initial binding poses of coproheme and monovinyl, monopropionyl deuteroheme. Coproheme in pose 0 reflects the correct binding of the substrate/redox cofactor in LmChdC (6FXJ) as reported in Figure 1. Monovinyl, monopropionyl deuteroheme in pose 90 corresponds to the intermediate structure proposed to be responsible for decarboxylation of p4. The Cβ atom of p2 is shown as a sphere.

p4 (involving 4 atoms) is 230 times higher in pose 90 compared to pose 0 (transfer via 13 atoms).

2.3. Reaction of Coproheme-LmChdC with H_2O_2 and Chlorite—Formation of Compound I and of the Y147 Radical. Upon addition of hydrogen peroxide to coproheme-LmChdC, decarboxylation of p2 and p4 leads to the formation of heme *b*-LmChdC. During this reaction the original electronic absorption spectrum of coproheme-LmChdC (Soret maximum: 393 nm) converts to a spectrum with the characteristics of heme *b*-LmChdC (Soret maximum: 410 nm). The reaction is slow, and the turnover number and k_{cat}/K_M values were determined to be ~0.0065 s^{-1} and 1.8 × 10^2 M^{-1} s^{-1} at pH 7.[5]

Hydrogen peroxide mediates the two-electron oxidation of ferric ChdC to a postulated (coproheme) compound I [oxoiron(IV) $Por^{\bullet+}$][6,11] which has not been trapped spectrophotometrically, most probably because of its fast conversion to compound I* [oxoiron(IV) $Y147^{\bullet}$]. Substitution of Y147 with alanine or histidine completely inactivates LmChdC (Figure 7C). Nevertheless, it was not possible to follow compound I formation by stopped-flow spectroscopy upon mixing of Y147A or Y147H with H_2O_2, most probably because of a decrease of in conformational stability and a structural rearrangement of the active site of those mutants, which impairs compound I formation by H_2O_2.[18] At high excess of hydrogen peroxide bleaching of coproheme was observed in Y147A and Y147H.

Other variant proteins (Y113A, R133A, M149A, K151A, R179A, Q187A, Y113A/K151A, M149A/Q187A, Y147A/R220A/S225A) were examined to assess the reaction with H_2O_2, but with the exception of K151A, Y147A, and Y147H, they had wild-type like catalytic activity. However, compound I formation was not observed for any. Most of these amino acids are involved in the extended H-bonding network of LmChdC involving the propionates p2, p4, p6, and p7 of coproheme.[18]

As it is known that chlorite also acts as a two-electron oxidant of heme proteins and mediates compound I formation similar to H_2O_2,[19−21] we tested whether chlorite is able to initiate the decarboxylation reaction of coproheme. Thus, we performed titrations analogous to the previously reported experiments using H_2O_2.[5] Interestingly, the spectral transitions of wild-type coproheme-LmChdC to heme *b*-LmChdC triggered by chlorite are identical to those mediated by H_2O_2 (Figure S1A). Moreover, the stoichiometry of the reaction is identical.[5] Plotting the normalized absorbance at 410 nm against the ratio of [chlorite]/[LmChdC] and fitting with a sigmoidal function, a midpoint of conversion at a [chlorite]/[LmChdC] ratio between 0.67 and 0.69 has been found. A 2-

DOI: 10.1021/acscatal.9b00963
ACS Catal. 2019, 9, 6766−6782

Table 2. Average Percentages of Hydrogen Bonds Per Propionate Per Monomer with Amino Acids in the Active Site during Simulation[a]

	coproheme (pose 90)				coproheme (pose 0)				monovinyl, monopropionyl deuteroheme, (pose 90)				monovinyl, monopropionyl deuteroheme, (pose 0)			
	p2	p4	p6	p7	p2	p4	p6	p7	p2	p4	p6	p7	p2	p4	p6	p7
S111			18	10		**60**		16			36	15				
Y113				19		32					43	34		**50**		
L114				**53**								46				
A115				49			7					33				
S116				**74**								26				
H117							2									
Y147		**80**			**98**					**74**						
K151			**83**			34					38			**94**		
W159						21					12			13		
H174		4														
R179	12						16									
S180	17															
Y181	13															
A182	17															
G183	40							35								6
Q187	**71**							**56**				3				28
W200			2			10								15		
S225		**66**			**95**					**89**						
F231		49			**57**					43						
Sum per propionate	168	199	103	205	250	157	25	107	0	205	129	156	0	171	0	34
Sum per ligand	675				540				489				206			

[a]The most frequently formed hydrogen bonds are in green, hydrogen bonds formed for more than 50% of the time are in bold. The p2 propionates do not exist in the three-propionate intermediate, thus the columns are in grey.

fold stoichiometric excess of chlorite or H_2O_2 is needed for completion of the conversion of coproheme to heme *b*. These findings support the proposed reaction mechanism that starts with the two-electron oxidation of ferric ChdC to compound I by either H_2O_2 or chlorite.

We also probed whether it is possible to monitor compound I formation of wild-type and mutant proteins mediated by chlorite. Neither mixing of wild-type LmChdC nor Y147A with chlorite gave reliable spectral and kinetic data. However, the variant Y147H allowed us to follow compound I formation spectrophotometrically at pH 7.0 (Figure 6A). Upon mixing of Y147H with chlorite, hypochromicity in the Soret region was observed with clear isosbestic points at 344, 425, 450, and 544 nm. Single wavelength measurements at the Soret maximum of coproheme were monophasic (for the first 0.5 s) and could be fitted by a single exponential function (Figure 6B). A pure compound I spectrum could not be observed due to a competing reaction, as evident from the relatively high intercept (2.5 s^{-1}). The competing reaction was identified as heme bleaching, due to pseudo-first-order conditions, as becomes evident when the reaction was followed for a longer time period (Figure S2). The linear dependence of k_{obs} as a function of chlorite concentration enabled the apparent bimolecular rate constant for compound I formation to be calculated, 1.2 × 10^4 M^{-1} s^{-1} at pH 7.0 (Figure 6C). Simulation of the data using the Pro-Kineticist software (Applied Photophysics) allowed calculating the coproheme compound I spectrum of Y147H with absorbance maxima at 391, 544, 583, and 645 nm (Figure 6D).

Compound I of LmChdC is rapidly converted to compound I* with the proposed formation of a catalytic tyrosyl radical ($Y147^{\bullet}$). In order to prove the existence of $Y147^{\bullet}$ during turnover of LmChdC, we used the spin trap 2-methyl-2-nitrosopropane (MNP), which is known to specifically attack and modify tyrosyl radicals yielding 3-nitrotyrosine.[22] Coproheme-LmChdC was treated with a large excess (83-fold) of hydrogen peroxide in the presence of MNP and was analyzed by mass spectrometry. LmChdC has 12 tyrosine residues (Figure 7). Upon mixing of coproheme-LmChdC with MNP in the absence of hydrogen peroxide, no modification of the tyrosine residues could be detected by mass spectrometry. In the presence of H_2O_2, only two out of the 12 tyrosine residues were modified by more than 1% (Figure 7A). Table 3 summarizes these data together with the calculated accessible surface areas of all tyrosines in LmChdC [$Å^2$, using the WHATIF server, based on the crystal structure for LmChdC

DOI: 10.1021/acscatal.9b00963
ACS Catal. 2019, 9, 6766−6782

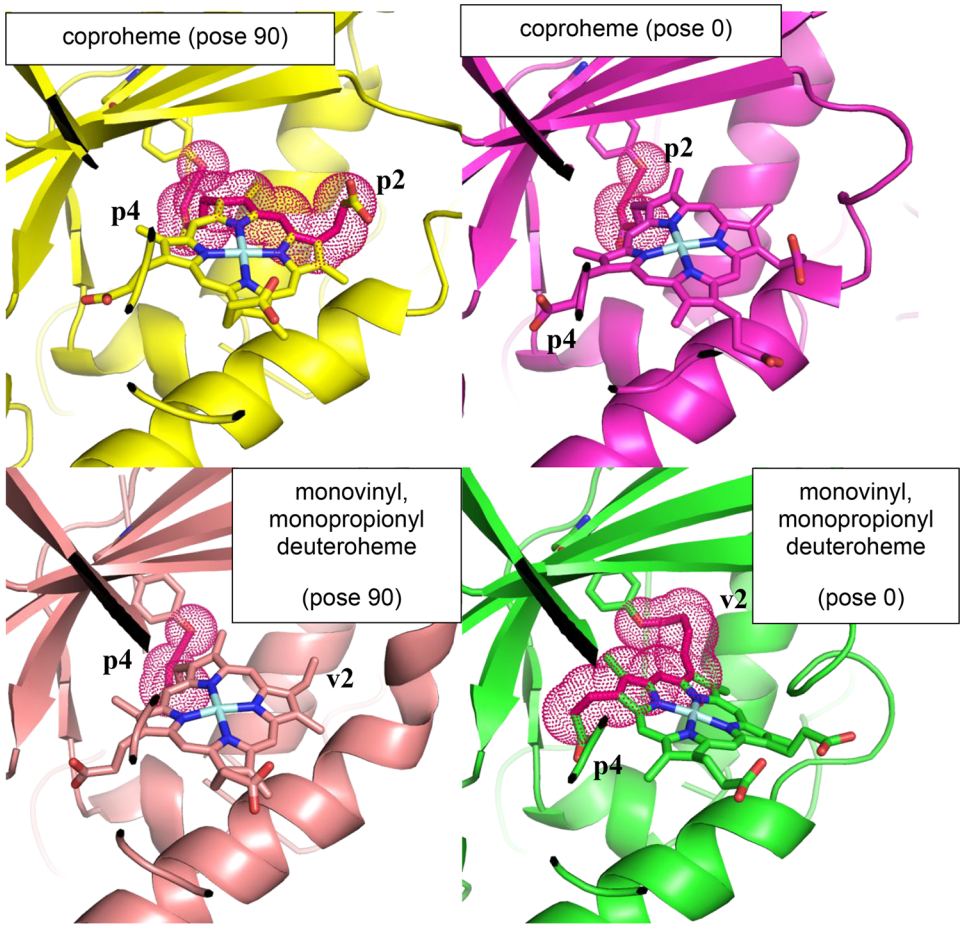

Figure 5. Proposed electron transfer pathways from p2 and p4 to Y147 for coproheme in poses 0 and 90 as well as from p4 to Y147 in monovinyl, monopropionyl deuteroheme in poses 0 and 90.

(6FXJ)]. The predicted catalytic Y147, which is not surface accessible, is modified by 56.04% and Y135 modified by 15.6%. The latter is located on the flexible loop at the access channel to the active site (Figure 7B).

2.4. Assignment of Propionyl Bands of Coproheme and Monitoring of the Conversion of Coproheme to Heme *b* by Resonance Raman Spectroscopy. The bending modes [$\delta(C_\beta C_c C_d)$] of propionate substituents are usually found in the low frequency region of the resonance Raman (RR) spectrum between 366 and 376 cm^{-1}. The frequencies correlate to the H-bond strength between the propionate and the nearby amino acids. Typically, the higher the number and the strength of the H-bonds, the higher the bending frequency and vice versa.[23] With the objective of assigning the four propionate bands of wild-type coproheme LmChdC, we analyzed the RR spectra of a series of mutants where the residues H-bonded with p2 (Y147, R220, and S225), p4 (Y113 and K151, the latter is also part of a H-bond network involving p2), p6 (R133 and R179, the latter is also H-bonded to the p7), and p7 (Q187) were replaced with alanine. As compared to the wild-type protein, decreasing of the H-bond strength is expected to result in a frequency downshift of the corresponding RR bending mode. However, as a consequence of the inhomogeneity of the H-bonds between the propionyls and residues in the five subunits (see Table S2) and the very extensive H-bond network spanning from p2 to p4 (see Figure 2A and B), it is impossible to predict the net effect on the frequency of each propionyl bending mode induced by the single, double, and triple mutation. Therefore, due to the inhomogeneous broadening following the loss of H-bonding interactions in the mutants and the severe overlapping of their frequencies, the assignment of the propionyl bending modes of the mutants involved in the H-bond interaction with p2 and p4 is less clear.

In the RR spectrum of wild-type coproheme-LmChdC at room temperature, only three propionate bending modes at 374, around 381 and 392 cm^{-1}, can be observed (Figure 8). In the complex of coproheme with the Y147A/R220A/S225A triple mutant a new band at 386 cm^{-1} can be identified (Figure 8, beige). This mutant lacks the H-bond interaction with the propionate group in position 2 (Figure 2 and Table 2). Therefore, this new band is tentatively assigned to the bending mode of a non-H-bonded p2, which in the wild-type protein is expected to have a higher frequency. Accordingly, an intensity increase in this region is also observed in the spectra of the coproheme mutants where the K151 residues interacting with propionate in position 2 have been replaced with Ala.

In the coproheme-Y113A complex, which lacks the H-bond interaction with the propionate in position 4 (Table 3), the band at 381 cm^{-1} (WT) downshifts to 379 cm^{-1} and increases in intensity (Figure 8, green). Consequently, this band is assigned to the bending mode of p4. Propionate in position 6 is directly H-bonded to R179 and, via a water molecule, to R133 (Table S1). In the coproheme-R179A complex the band at 374 cm^{-1} (wild-type LmChdC) unexpectedly upshifts to 377 cm^{-1} (Figure 8, brown), suggesting that a strengthening of

DOI: 10.1021/acscatal.9b00963
ACS Catal. 2019, 9, 6766−6782

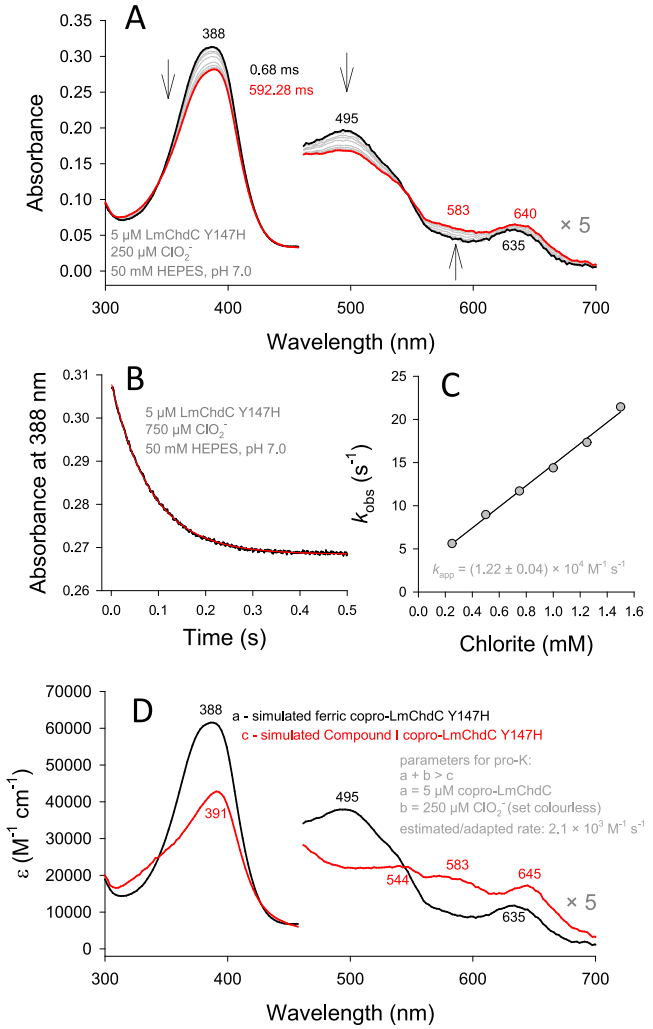

Figure 6. Formation of compound I of LmChdC Y147H mediated by chlorite. (A) Spectral transitions upon mixing of 5 μM LmChdC with 250 μM chlorite at pH 7.0 (50 mM HEPES). The black spectrum was obtained after 0.68 ms. Gray spectra were taken at 11.6, 33.3, 59.2, 104.7, 208.8, 306.0, 406.6, and 514.8 ms; the final depicted spectrum is shown in red (after 592.3 ms). (B) Experimental time trace (black) and single exponential fit (red) monitored at 388 nm obtained upon mixing of 5 μM LmChdC Y147H with 750 μM chlorite. (C) Linear dependence of k_{obs} values on the chlorite concentration. (D) Simulation of the spectra shown in part A using Pro-K software and calculation of the spectrum of compound I.

the H-bond interactions occurs after mutation. By contrast, the frequency is unchanged in the coproheme-R133A complex spectrum.

The mutant Q187A involves a residue which interacts only with p7 (Table 3). In its coproheme complex the band at 392 cm^{-1} (wild-type LmChdC) downshifts to 389 cm^{-1}(Figure 8, light blue) and is, therefore, assigned to the p7 bending mode. The spectrum of the coproheme-M149A/Q187A double mutant complex is roughly an average of the coproheme-M149A and coproheme-Q187A spectra.

Based on these findings the three propionate bending modes of wild-type coproheme-LmChdC at room temperature can be assigned to p6 (374 cm^{-1}), p4 (381 cm^{-1}), and p7 (392 cm^{-1}). As noted above, the corresponding bending of p2 is expected at a frequency higher than 386 cm^{-1}. It has to be noted that a new band at 412 cm^{-1} (in the region of the vinyl bending modes) appears in the spectra of the coproheme-Y147A/R220A/S225A, coproheme-Y113A/K151A, and coproheme-K151A complexes which are mainly a 6cLS (six-coordinate low spin) form (data not shown). Since these species are catalytically inactive (see above), they cannot form a heme *b* complex, and consequently no band due to vinyl bending modes is expected. Therefore, the origin of the band at 412 cm^{-1}, which appears only in the 6cLS complex spectra, remains unclear.

In order to increase the spectral resolution, we performed RR measurements at 80 K, since the band widths decrease as the temperature is lowered. As reported in the Experimental Section, the experiments have been obtained with the 413.1 nm excitation to avoid the plasma lines of the 406.7 nm excitation wavelength in the low frequency region. At 80 K, the wild-type LmChdC spectrum shows four well-defined bands at 374, 383, 389, and 399 cm^{-1} (Figure 9). However, unlike the wild-type protein, no clear assignment of the propionyls in the mutant proteins could be obtained at 80 K. The spectra showed multiple changes induced by the temperature. First, as previously found, heme proteins undergo a temperature-induced transition from high to low spin.[24−27] At low temperature the amount of 6cLS increases and becomes the main species (Figure S3). As a consequence, the band at 414 cm^{-1} becomes very strong and is also observed in the coproheme complexes of M149A, Y113A, R179A, and R133A (Figure S4). Moreover, an upshift of the p2 bending mode is observed in those mutants involved in the extensive H-bond network spanning from p4 to p2 suggesting a strengthening of the H-bond interaction induced by the low temperature.

The assignment of the bending modes of the propionates in positions 6 and 7 is also confirmed by the spectra of the heme *b* complexes. In fact, upon conversion of coproheme into heme *b*, the propionate groups in positions 2 and 4 are decarboxylated into vinyl groups, leaving only the propionates in positions 6 and 7. At room temperature, in wild-type heme *b*-LmChdC the two bands at 378 and 392 cm^{-1} are due to the $[\delta(C_\beta C_c C_d)]$ propionate bending modes. The broad band centered at 418 cm^{-1} derives from the two overlapping $[\delta(C_\beta C_a C_b)]$ vinyl bending modes. The presence of two vinyl bending modes, collapsed into one broad band, is confirmed by the presence of two vinyl stretching modes at 1621 and 1632 cm^{-1} in the RR high frequency region spectrum at 298 K (Figure 10, red spectrum).

As compared to the wild-type coproheme-complex, the p6 frequency of wild-type heme *b*-LmChdC is 4 cm^{-1} upshifted, suggesting altered surroundings that cause a strengthening of the hydrogen bonding to p6. By contrast, the frequency of p7 remains unchanged. As previously observed for wild-type coproheme LmChdC, lowering the temperature does not affect the p6 frequency of heme *b*-LmChdC (which remains at 378 cm^{-1}) whereas it causes a ∼ 7 cm^{-1} upshift of the p7 band (from 392 to 399 cm^{-1}).

The frequencies (cm^{-1}) and assignments of the propionate $[\delta(C_\beta C_c C_d)]$ bending modes obtained at 298 and 80 K for the WT are reported in Table 4.

Figure 11 compares the heme *b* RR spectra of wild-type LmChdC and selected mutants obtained at 298 (left) and 80 K (right). At room temperature, the propionate bands of heme *b*-M149A are unaffected by mutation, as expected, while the vinyl bending modes are centered at 415 cm^{-1}, 3 cm^{-1} downshifted compared to the wild-type protein. In the heme *b*-R179A and heme *b*-R133A spectra a 4 cm^{-1} upshift of the p6

DOI: 10.1021/acscatal.9b00963
ACS Catal. 2019, 9, 6766−6782

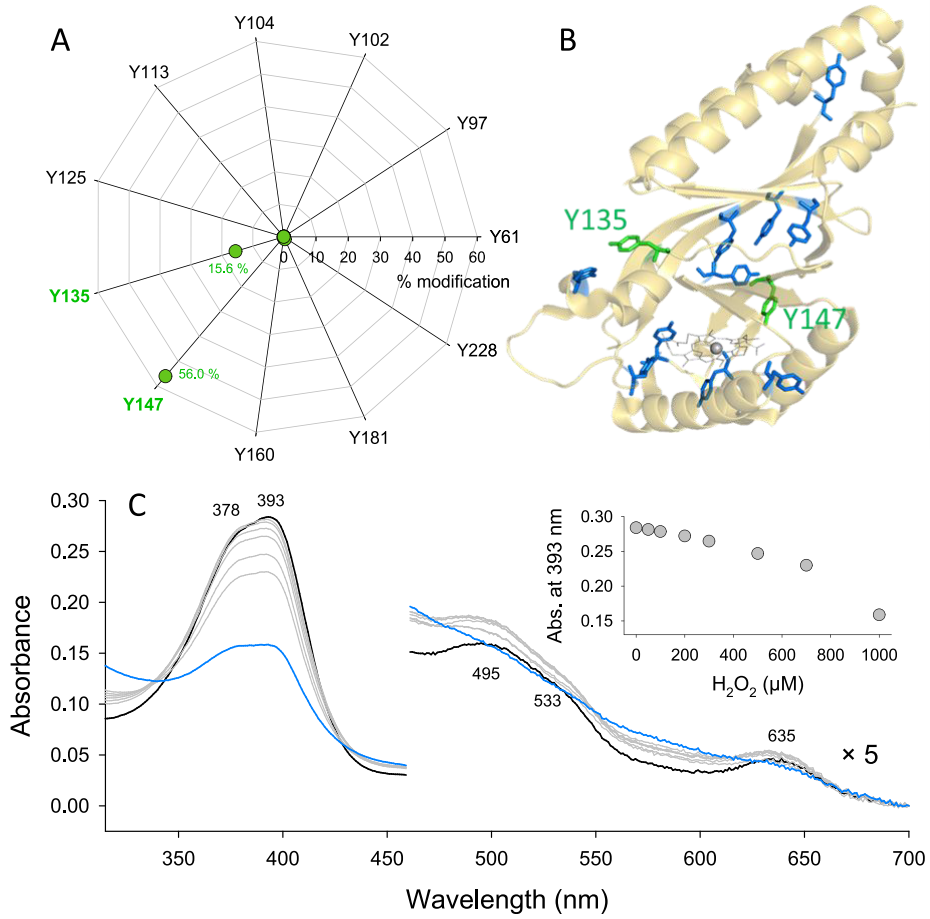

Figure 7. Identification of catalytic Y147 of LmChdC by spin-trapping using 2-methyl-2-nitrosopropane. (A) Identified modified tyrosine residues obtained by treatment of LmChdC with excess H_2O_2 in the presence of the spin trap MNP followed by mass spectrometric analysis. (B) Presentation of subunit A of LmChdC as yellow cartoon; tyrosines are shown as sticks. Unmodified tyrosines are depicted in blue, whereas 3-nitrotyrosines are depicted in green. (C) Titration of Y147A with hydrogen peroxide in 50 mM phosphate buffer pH 7.0.

Table 3. Tyrosyl Radicals in LmChdC[a]

tyrosine residue	accessible surface area (Å^2)	% modified (+46 Da)
Y61	0.1057	0.12
Y97	8.4632	0.00
Y102	19.4741	0.00
Y104	0.3495	0.00
Y113	1.3375	0.00
Y125	23.9246	0.00
Y135	16.1367	15.60
Y147	**0.0000**	**56.04**
Y160	1.4756	0.30
Y181	5.3286	0.80
Y198	16.2791	n.d.[b]
Y228	0.6343	0.00

[a]A 30 μM portion of LmChdC, preincubated with excess MNP, was treated with 2.5 mM H_2O_2, and covalent modifications were identified using mass spectrometry. [b]Not detected.

band from 378 (wild-type) to 382 cm^{-1} is observed, similarly to the coproheme-R179A complex [where the band upshifts 3 cm^{-1}, from 374 (wild-type) to 377 cm^{-1}], while a 2 cm^{-1} downshift is observed in the frequency of p7 in both heme *b*-R179A and heme *b*-Q187A spectra. At low temperature, the vinyl bending modes are observed at 417 cm^{-1} (414 cm^{-1} in the heme *b*-M149A) and at about 407 cm^{-1}. Unfortunately, due to the very high fluorescence background we were unable to collect the RR spectra in the high frequency region at 80 K, but the stretching modes at 1621 and 1632 cm^{-1} observed in the RR spectra at 298 K (Figure 10) are consistent with the bending modes at 407 and 417 cm^{-1}, respectively.[28,29]

Finally, in order to obtain better insight into the catalytic mechanism, we followed the conversion of coproheme into heme *b* by titrating the coproheme-M149A complex with hydrogen peroxide. We performed the titration with this mutant, because the coproheme-M149A complex is much less fluorescent than that of the wild-type protein, thus allowing better resolution of the propionate bands. Moreover, the heme *b*-M149A and heme *b*-wild-type protein spectra are identical in the propionate region, the only difference being the frequency of the broad vinyl band, as described above.

Figures 12 and 13 show the titration of coproheme-M149A with hydrogen peroxide followed by UV−vis (298 K) and RR (80 K) spectroscopy. Initially, the addition of hydrogen peroxide causes a decrease of the 6cLS species of the coproheme complex, as indicated by the decrease of the Soret band at 406 nm in the second derivative spectrum and the blue shift of the maximum in the UV−vis spectrum (Figure 12, spectra a, b). In spectrum c the 6cLS species of the heme *b* complex becomes clearly evident by the red shift of the Soret maximum from 396 to 401 nm and the increase of a band at 407 nm in the D^2 spectrum. This species increases as the

DOI: 10.1021/acscatal.9b00963
ACS Catal. 2019, 9, 6766−6782

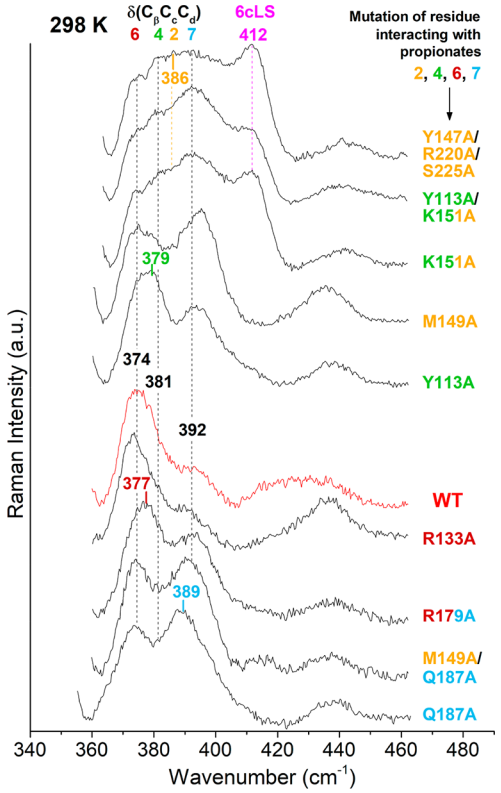

Figure 8. Comparison of resonance Raman spectra in the low frequency region of the coproheme-LmChdC complexes of the WT and mutants obtained at 298 K (λ_{exc} 406.7 nm). The bands tentatively assigned to the bending modes $\delta(C_\beta C_c C_d)$ of the propionate groups in position 2, 4, 6, and 7 are reported in beige, green, brown, and light blue, respectively. Accordingly, the label color of the mutants indicates the propionate group with which the mutated residues interact. In magenta the band corresponding to the 6cLS (six-coordinate low spin) species is depicted. The spectrum of wild-type coproheme-LmChdC is reported in red. The spectra have been shifted along the ordinate axis to allow better visualization. Experimental conditions: laser power at the sample 5 mW, average of 8 spectra with a 80 min integration time (Q187A); average of 12 spectra with a 120 min integration time (M149A/Q187A); average of 10 spectra with a 100 min integration time (R179A and R133A); average of 15 spectra with 150 min integration time (WT); average of 9 spectra with a 90 min integration time (Y113A, M149A, and K151A); average of 12 spectra with a 120 min integration time (Y113A/K151A and Y147A/R220A/S225A).

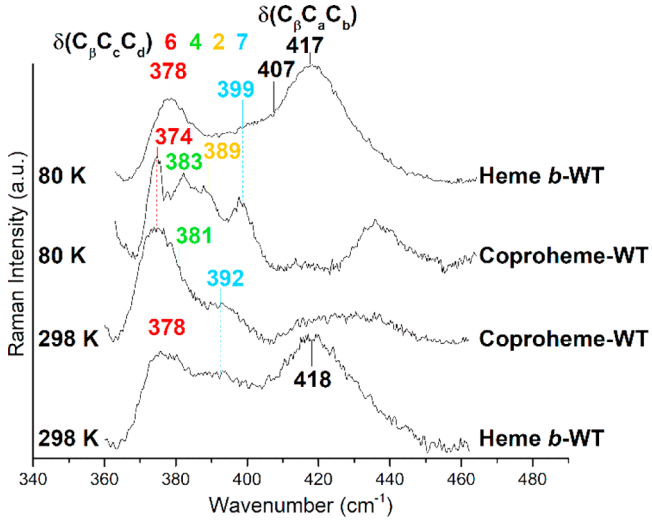

Figure 9. Comparison of resonance Raman spectra in the low frequency region of wild-type coproheme-LmChdC and wild-type heme *b*-LmChdC obtained at 298 K (λ_{exc} 406.7 nm) and at 80 K (λ_{exc} 413.1 nm). The bands tentatively assigned to the bending modes $\delta(C_\beta C_c C_d)$ of the propionate groups in positions 2, 4, 6, and 7 are reported in beige, green, brown, and light blue, respectively. The bending modes $\delta(C_\beta C_a C_b)$ of the vinyl groups are also shown. The spectra have been shifted along the ordinate axis to allow better visualization. Experimental conditions: laser power at the sample 5 mW, average of 15 spectra with 150 min integration time (298 K), and laser power at the sample 10 mW, average of 5 spectra with 100 min integration time (80 K).

titration proceeds leading to a red-shift of the Soret band until reaching its final form, characterized by a Soret band at 411 nm (412 in the D_2 spectrum). The apparent lack of a spectrum representing the three-propionate intermediate is in agreement with previously published titrations, which were followed by both UV−vis spectroscopy and mass spectrometry.[5] This is probably due to the overlap of the isosbestic point and the maximum of the Soret band of the three-propionate intermediate which is at 398 nm.[4]

As previously discussed (Figure 9), a distinctive difference between the coproheme and heme *b* complexes is the p6 band frequency, which upshifts from 374 cm^{-1} (coproheme complex) to 378 cm^{-1} (heme *b* complex). The formation of the heme *b* band is clearly observed during the titration, since addition of hydrogen peroxide to the coproheme-M149A complex causes a progressive broadening of the band at 374 cm^{-1}(Figure 13, spectra b−d), with the concomitant decrease of the p2 band at 394 cm^{-1}. Conversely, the p7 band at 399 cm^{-1} does not change. Due to the upshift of the p6 band, it is impossible to follow the disappearance of the p4 band at 383 cm^{-1}. The formation of two vinyls highlighted by the appearance of the two bending modes at 407 and 414 cm^{-1} is clearly observed.

3. DISCUSSION

To date only one crystal structure (5LOQ) has been available of an iron coproporphyrin III (coproheme)-bound coproheme decarboxylase, namely from *Listeria monocytogenes* (LmChdC).[5] Only two out of the four propionate groups of coproheme in chains A and D showed clear electron densities, whereas the other two positions were unresolved and, therefore, presumed to be highly flexible. A second structure of a manganese coproporphyrin III from GsChdC,[6] which is unreactive toward hydrogen peroxide,[12] was solved (5T2K) showing a different (i.e., 90° rotated) orientation of coproheme and clear electron densities for the propionates.[6] Coproheme can be slowly converted to the three propionate intermediate and further to heme *b* by oxygen activation.[12] Thus, we revisited the structure of coproheme-LmChdC (5LOQ) and solved the crystal structure of the inactive (cyanide-blocked) resting state (6FXJ). The active site architecture of the structure (Figure 1) is very similar to that of manganese coproheme-GsChdC, allowing us to resolve the propionyls p2, p4, and p6.

Based on presently available knowledge, it is very likely that, in the absence of cyanide, coproheme in the previously reported structure of LmChdC (5LOQ) was partially converted to the three-propionate intermediate, containing, therefore, p2 partially decarboxylated to a vinyl substituent. On

DOI: 10.1021/acscatal.9b00963
ACS Catal. 2019, 9, 6766−6782

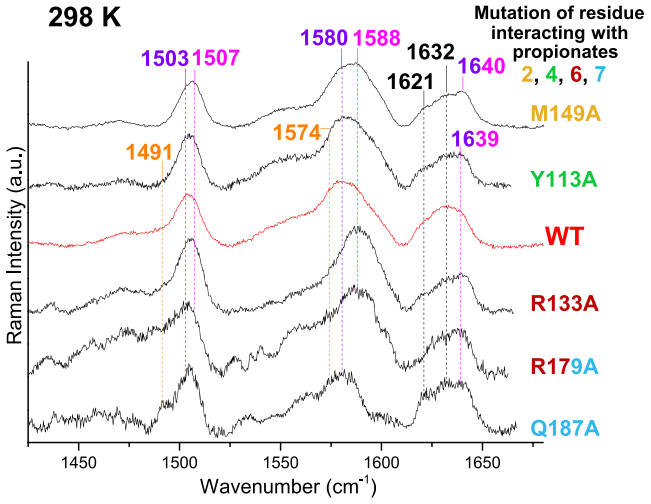

Figure 10. Resonance Raman spectra in the high frequency region of wild-type heme *b*-LmChdC complexes and mutant heme *b* complexes obtained at 298 K (λ_{exc} 413.1 nm). The band wavenumbers in magenta indicate the His174-Fe-Gln187 6cLS species,[10] those in violet indicate the 6cLS species with an unknown N-residue as the sixth ligand, and those in orange show a minor 5cHS (five-coordinate high spin) species. The mutant label colors beige, green, brown, and light blue indicate the positions 2, 4, 6, and 7, respectively, of the propionate groups with which the mutated residues interact. The spectrum of the wild-type heme *b* complex is reported in red. The spectra have been shifted along the ordinate axis to allow better visualization. Experimental conditions: laser power at the sample 5–10 mW, average of 13 spectra with 130 min integration time (Q187A); average of 7 spectra with 70 min integration time (R179A); average of 6 spectra with 120 min integration time (R133A); average of 6 spectra with a 30 min integration time (wild-type); average of 5 spectra with 50 min integration time (Y113A); average of 10 spectra with 100 min integration time (M149A).

Table 4. Frequencies (cm^{-1}) and Assignments of the Propionate [$\delta(C_\beta C_c C_d)$] Bending Modes Obtained at 298 K[a]

	p2	p4	p6	p7	
WT	389	381 (383)	374	392 (399)	
Y147A/R220A/S225A	386	381	374	392	p2
K151A/Y113A	386	381	374	392	p2/p4
K151A	386	381	374	392	p2/p4
M149A	389	381	374	392	p2
Y113	389	379	374	392	p4
R133	389	381	374	392	p6
R179	389	381	377	392	p6/p7
Q187	389	381	374	389	p7

[a]In brackets the frequencies observed at 80 K for the WT are reported. The color coding of the four propionate groups corresponds to that used in the RR figures.

this basis, we built a new and improved model (6FXQ) from the 5LOQ data containing both coproheme and the three-propionate intermediate (monovinyl, monopropionate deuteroheme). We performed further refinement, resulting in better statistics (Table 1). The active site in the new model (6FXQ) is characterized by two porphyrin species having occupancies of 50% each: coproheme in the resting state orientation [corresponding to the newly solved coproheme-LmChdC structure (6FXJ)] and the three propionate intermediate being rotated by 90°, thus bringing p4 in close proximity to the catalytic Y147. Such an orientation eliminates the need for (i) a (postulated) long-range electron transfer from p4 in its original position to Y147 and (ii) the presence of a second reaction site within the same cavity. Generally, enzymes with two active sites usually have regulatory tasks and catalyze reverse or consecutive reactions.[30−32] Several FAD-dependent enzymes (e.g., pyranose dehydrogenase) were proposed to have two His residues at the active site that both act as general bases in the reductive half reaction, but later this was demonstrated to be wrong.[33−35] The hypothesis of two general bases was intriguing in the case of pyranose dehydrogenase, which oxidizes various mono- and oligosaccharides at different positions (C1 and C4). The observed substrate specificity was subsequently explained by reorientation/rotation of the substrate itself.[33] Similar substrate dynamics were described for the enzyme pectin methylesterase.[36]

Scheme 1 depicts the rotation of the redox cofactor after the first decarboxylation step underlining the role of Y147 in LmChdC as the only site of decarboxylation for both p2 and p4, as also supported by recently published spectroscopic studies.[11] Scheme 1 nicely demonstrates how during turnover (i.e., conversion of coproheme to heme *b*) the surroundings of the (remaining) propionates change with alteration of the H-bonding partner. The proposed rotation of the three-propionate cofactor is also supported by analysis of the dynamics of H-bonding interactions of both coproheme and the three-propionate intermediate in different poses. MD simulations suggest that the monovinyl, monopropionyl deuteroheme with p4 close to Y147 forms more than twice as many H-bonds compared to the unrotated orientation. Moreover, the probability of electron transfer from Cβ of p4 to the terminal oxygen of Y147 is shown to be 230 times higher when p4 is in the rotated orientation and thus close to Y147.

Scheme 1 is also supported by the RR studies. We analyzed the RR spectra of wild-type coproheme-LmChdC and heme *b*-LmChdC and a series of mutants where the residues H-bonded with p2/v2, p4/v4, p6, and p7 were replaced with alanine. The bending modes of all four propionyl substituents of coproheme and v2, v4, p6, and p7 in heme *b* have been assigned (Table 4), and we were able to follow the spectral transition of coproheme to heme *b* mediated by hydrogen peroxide. The data clearly show that the p6 frequency (present in both coproheme and heme *b*) upshifts by 4 cm^{-1} in heme *b*-LmChdC as compared to coproheme-LmChdC, suggesting a change in the H-bonding interaction with the residues in the heme cavity as compared to the coproheme complex. Inspection of the 6FXJ structure and Scheme 1 shows that p6 in the rotated orientation interacts with the Y113 and K151 residues, similar to p4 in coproheme-LmChdC (whose bending mode is assigned to the band at 381 cm^{-1}). The p7 frequency in coproheme-LmChdC and heme *b*-LmChdC is identical, which reflects the solvent exposure of p7 in the (coproheme) resting state and the (three-propionate) rotated orientation (Table S3).

The question of whether the monovinyl intermediate stays bound and rotates within the active site or whether it is released after the first decarboxylation and rebinds in a different orientation remains unanswered. The active site volume would allow a rotation in the bound state, but there are also indications favoring the release-and-rebinding mechanism. During the enzymatic reaction significantly greater than stoichiometric amounts of the three-propionate intermediates were detected in previous studies.[2,37] This would only be

DOI: 10.1021/acscatal.9b00963
ACS Catal. 2019, 9, 6766−6782

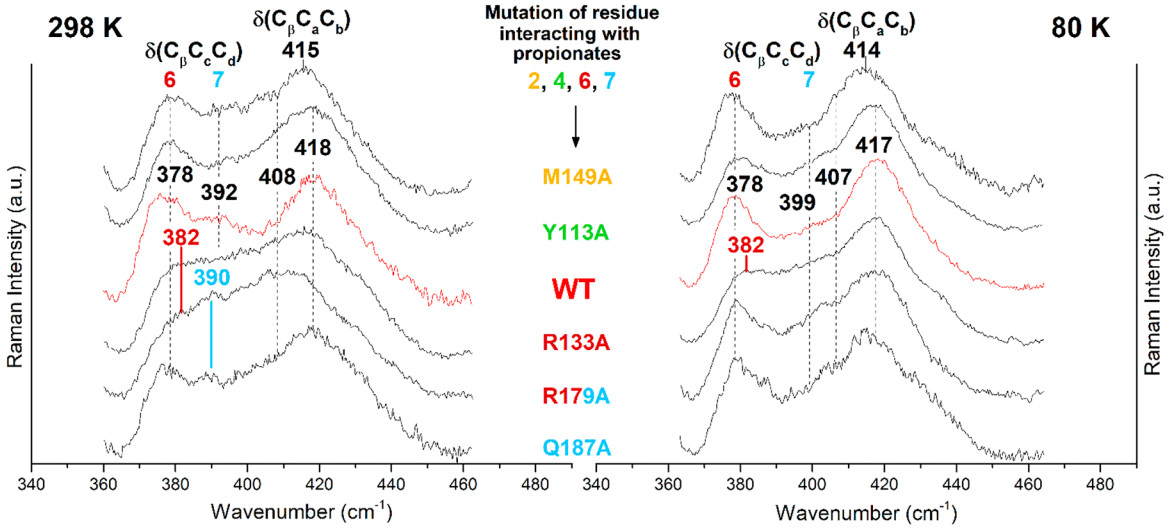

Figure 11. Comparison of resonance Raman spectra in the low frequency region of wild-type heme *b*-LmChdC and mutant heme *b* complexes obtained at 298 K (left) and 80 K (right) (both λ_{exc} 413.1 nm). The bands tentatively assigned to the bending modes $\delta(C_\beta C_c C_d)$ of the propionate groups in positions 6 and 7 are reported in brown and light blue, respectively. Accordingly, the mutant label colors beige, green, brown, and light blue indicate the positions 2, 4, 6, and 7, respectively, of the propionate group/s with which the mutated residues interact. The bending modes $\delta(C_\beta C_a C_b)$ of the vinyl groups are also shown. The spectrum of the heme *b*-WT complex is reported in red. The spectra have been shifted along the ordinate axis to allow better visualization. Experimental conditions: (298 K) laser power at the sample 5−10 mW, average of 13 spectra with a 130 min integration time (Q187A); average of 10 spectra with a 200 min integration time (R179A); average of 9 spectra with a 180 min integration time (R133A); average of 4 spectra with 40 min integration time (WT); average of 4 spectra with a 80 min integration time (Y113A); average of 12 spectra with a 120 min integration time (M149A). (80 K) laser power at the sample 10 mW, average of 9 spectra with a 180 min integration time (Q187A, R179A and Y113A); average of 10 spectra with a 200 min integration time (R133A); average of 16 spectra with 320 min integration time (WT); average of 6 spectra with a 120 min integration time (M149A).

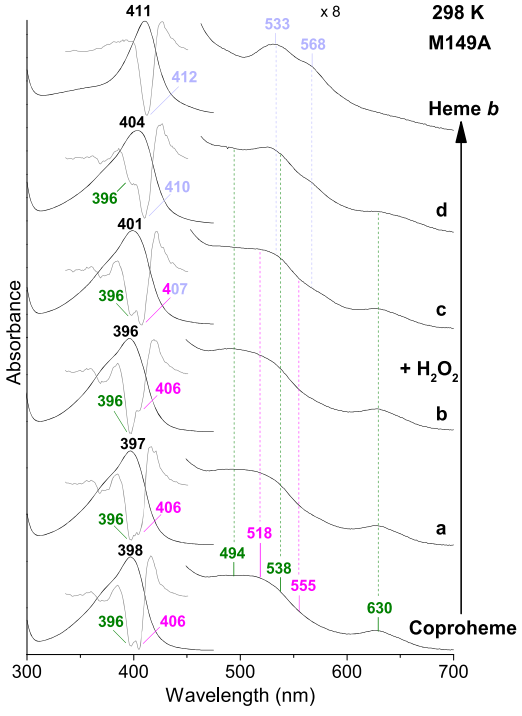

Figure 12. UV−vis absorption and second derivative (D^2) spectra of the coproheme-M149A complex titrated at 298 K with hydrogen peroxide until complete conversion into the heme *b*-M149A complex. The band wavelengths assigned to the 5cQS (quantum mechanically mixed-spin state), 6cLS of the coproheme complex and 6cLS of the heme *b* complex are indicated in olive green, magenta, and light violet, respectively. The spectra have been shifted along the ordinate axis to allow better visualization. The 450−700 nm region is expanded 8-fold.

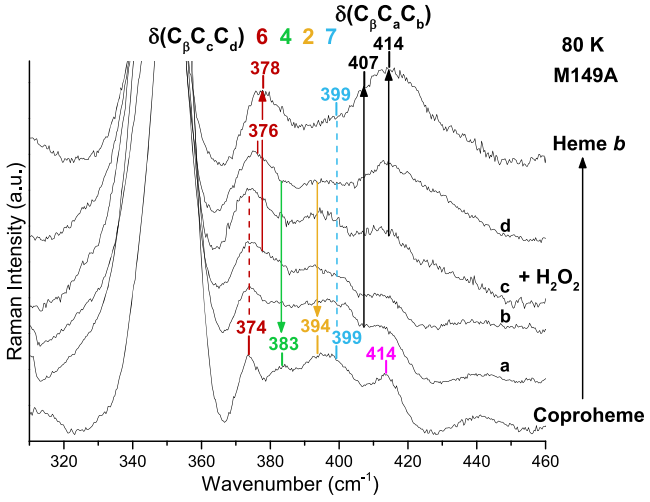

Figure 13. Resonance Raman spectra in the low frequency region obtained at 80 K (λ_{exc} 413.1 nm) of coproheme−M149A titrated with hydrogen peroxide until complete conversion into heme *b*-M149A. The bands tentatively assigned to the bending modes $\delta(C_\beta C_c C_d)$ of the propionate groups in positions 2, 4, 6, and 7 are reported in beige, green, brown, and light blue, respectively. The bending modes $\delta(C_\beta C_a C_b)$ of the vinyl groups are reported in black. The band due to the 6cLS species is reported in magenta. The spectra have been shifted along the ordinate axis to allow better visualization. Experimental conditions: laser power at the sample 10 mW, average of 6 spectra with a 120 min integration time (each spectrum).

possible if the substrate is released after the first decarboxylation.

Complete conversion of coproheme to heme *b* requires two hydrogen peroxide molecules. Except for Y147A and K151A,

DOI: 10.1021/acscatal.9b00963
ACS Catal. 2019, 9, 6766−6782

Scheme 1. Orientations and Surroundings of Coproheme, Three-Propionate Intermediate, and Heme *b* of LmChdC during the Whole Reaction Cycle[a]

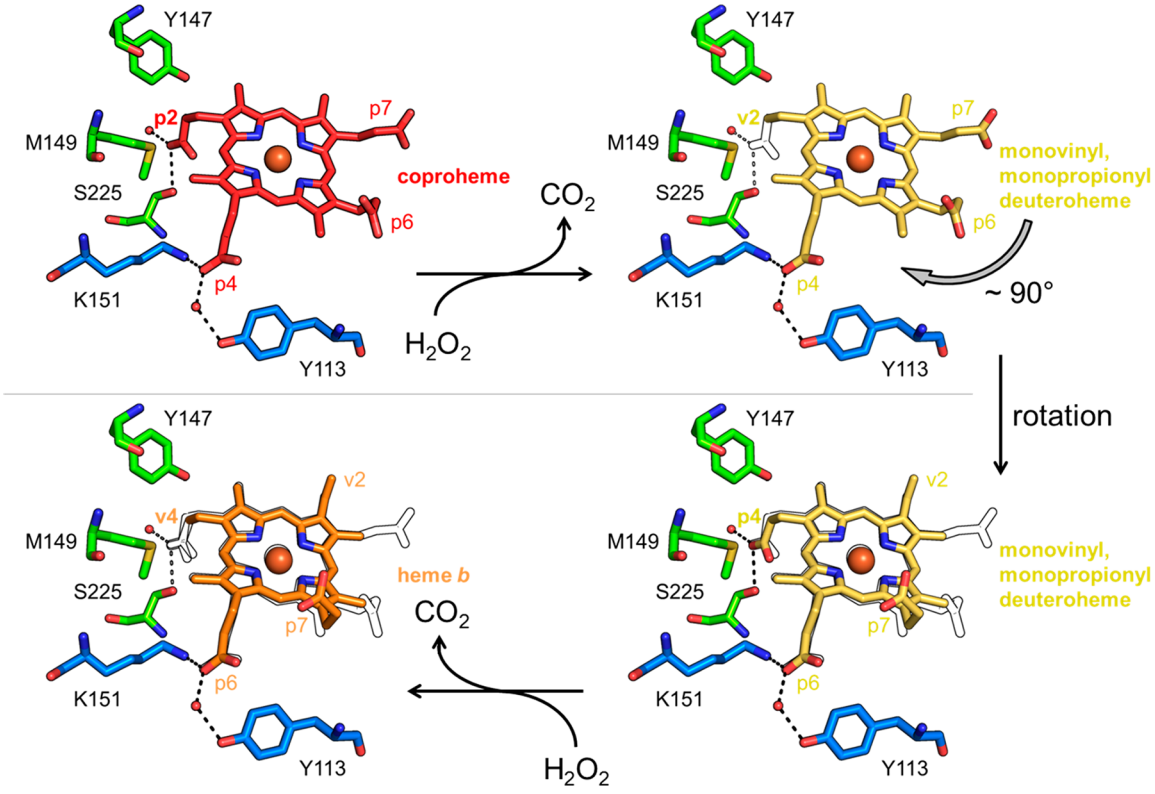

[a]The first decarboxylation step is initiated by oxidation of ferric coproheme-LmChdC by hydrogen peroxide. Propionate at position 2 is decarboxylated, and the resulting three-propionate intermediate is rotated by 90°, thereby bringing p4 close to Y147. A second hydrogen peroxide molecule is necessary for decarboxylation of p4. The scheme also depicts the H-bonding interactions of coproheme in the resting state as well as of the three-propionate intermediate in the rotated orientation.

all LmChdC variants exhibit a wild-type-like catalytic activity.[18] During decarboxylation of the first propionate substituent, H_2O_2 oxidizes coproheme-LmChdC to compound I [oxoiron-(IV) Por$^{\bullet+}$], which rapidly converts to compound I* [oxoiron(IV) $^{\bullet}$Y147]. This species attacks the Cβ atom of the corresponding propionate. Upon using the spin trap MNP, we could clearly demonstrate that Y147 is catalytically essential and oxidized during turnover, which fully supports data from SaChdC and the role of homologous Y145.[6] This also further suggests that this mechanism is valid for the entire Clade 1 of ChdCs.[12]

Upon elimination of Y147, which renders LmChdC completely inactive, the conversion of compound I to compound I* is suppressed. Moreover, we demonstrated that chlorite is a better two-electron oxidant of LmChdC compared to H_2O_2, and mediated rapid decarboxylation of coproheme (Figure S1). By using chlorite as oxidant we were able to trap the compound I state of LmChdC and succeeded in monitoring the conversion of ferric coproheme-Y147H to the coproheme compound I state. For the first time the kinetics of formation and the spectral signatures of a coproheme compound I could be monitored.

Compound I formation of ChdC must be the rate-limiting step during turnover since the hydrophobic distal cavity lacks a base for deprotonation of H_2O_2. This is consistent with the solvent deuterium isotope effect on the reaction rate of ChdC with H_2O_2.[7] By contrast, ClO_2^- is always deprotonated under reaction conditions due to its low pK_a value and rapidly binds to ferric coproheme. Nevertheless, chlorite is definitely not present in the physiological environment and can be excluded as the natural oxidant for ChdCs. Hydrogen peroxide is always available in biological fluids, but its reactivity with ChdCs is rather low and inefficient. Consequently, ChdCs are prone to heme bleaching in the presence of excess hydrogen peroxide.[5,12] We have recently shown that promotion of a closed conformation of LmChdC is triggered by the distal mobile Q187. This could play an important role in compound I formation.[10,18] Upon disrupting the H-bonding network between p2 and p4 or elimination of Q187, formation of an open conformation has been observed and catalytic activity was diminished.[10]

In summary, by combining our data with that of the literature a consensus reaction mechanism for decarboxylation of coproheme by ChdCs can be proposed (Scheme 2). Upon reaction with chlorite/H_2O_2, a coproheme-compound I [oxoiron(IV) Por$^{\bullet+}$] is formed and oxidizes Y147 to yield a tyrosyl radical [compound I*, i.e oxoiron(IV) $^{\bullet}$Y147]. The tyrosyl radical then abstracts a hydrogen atom (H$^{\bullet}$) from the β-carbon of p2, followed by migration of the unpaired propionyl electron to the redox cofactor and reduction of the oxoiron(IV) species to the ferric state. Concomitantly the substituent is stabilized by elimination of carbon dioxide thereby forming the vinyl substituent at position 2.

After decarboxylation of p2, the three propionate intermediate is rotated by 90° and a monovinyl, monopropionate deuteroheme-compound I and compound I* is formed by a

DOI: 10.1021/acscatal.9b00963
ACS Catal. 2019, 9, 6766−6782

Scheme 2. Molecular Radical Mechanism of Coproheme Decarboxylation in ChdC[a]

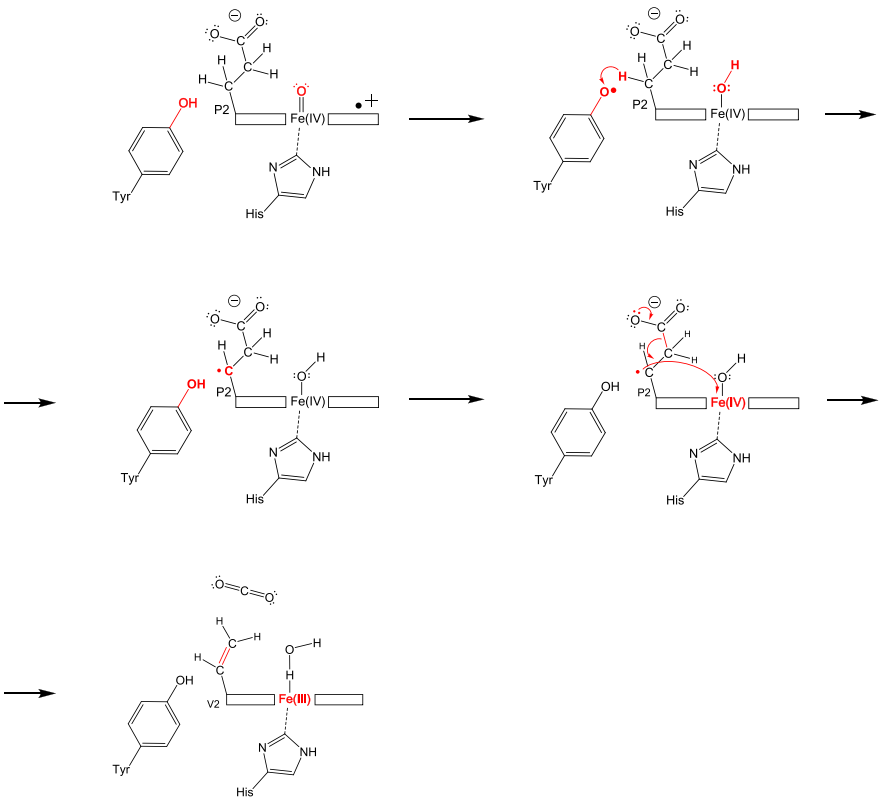

[a]Oxidation of ferric coproheme ChdC by hydrogen peroxide or chlorite forms compound I [oxoiron(IV) Por$^{\bullet+}$] which is rapidly converted to compound I* [oxoiron(IV) $^{\bullet}$Y147]. The tyrosyl radical attacks Cβ of the propionate at position 2 (p2) and abstracts a hydrogen atom (H$^{\bullet}$). Migration of the formed unpaired propionyl electron to the redox cofactor forms the ferric state, whereas the substituent is stabilized by elimination of carbon dioxide thereby forming the vinyl substituent at position 2. After p2 decarboxylation, the three propionate intermediate is rotated by 90° forming a monovinyl, monopropionate deuteroheme-compound I, and subsequently, compound I* is formed by a second H_2O_2 molecule (Schemes 1 and 2). The $^{\bullet}$Y147 radical now attacks p4 following the same sequence of reactions.

second H_2O_2 molecule (Schemes 1 and 2). Subsequently, p4 is attacked by $^{\bullet}$Y147 and the second decarboxylation reaction follows the same sequence as described above (Scheme 2). The extensive hydrogen bonding network of p2 and p4 supports the proposed mechanism including the rotation of the cofactor after the first decarboxylation step. Upon elimination of K151 LmChdC is almost completely inactive. The crystal structures of coproheme-LmChdC and the three-propionate intermediate clearly demonstrate that K151 plays an important role in stabilizing both coproheme and the three-propionate intermediate. It provides H-bonding to p2 (via two waters) and p4 of coproheme, but it also stabilizes p4 and p6 in the (rotated) intermediate structure. The RR data of heme *b*-LmChdC have clearly shown that p6 in heme *b*-LmChdC makes stronger H-bonding interactions compared to p6 in the coproheme form, thus supporting the proposed mechanism. Unfortunately, the crystal structure of a heme *b*-ChdC is still missing, but crystallization trials with ChdCs from various organisms are in progress.

■ ASSOCIATED CONTENT

Supporting Information

The Supporting Information is available free of charge on the ACS Publications website at DOI: 10.1021/acscatal.9b00963.

Full experimental details and additional figures and tables discussed in the text (PDF)

■ AUTHOR INFORMATION

Corresponding Authors

*E-mail: giulietta.smulevich@unifi.it. Phone: +39 055 4573083.

*E-mail: stefan.hofbauer@boku.ac.at. Phone: +43-1-47654-77258. Fax: +43-1-47654-77059.

ORCID

Chris Oostenbrink: 0000-0002-4232-2556

Paul G. Furtmüller: 0000-0002-1199-2469

Christian Obinger: 0000-0002-7133-3430

Giulietta Smulevich: 0000-0003-3021-8919

Stefan Hofbauer: 0000-0003-3375-7715

Notes

The authors declare no competing financial interest.

■ ACKNOWLEDGMENTS

This project was supported by the Austrian Science Fund, FWF [Doctoral program BioToP—Molecular Technology of Proteins (W1224) and the project P29099]. We thank Dr. B. D. Howes for helpful discussion.

■ REFERENCES

(1) Dailey, H. A.; Dailey, T. A.; Gerdes, S.; Jahn, D.; Jahn, M.; O'Brian, M. R.; Warren, M. J. Prokaryotic Heme Biosynthesis: Multiple Pathways to a Common Essential Product. *Microbiol Mol. Biol. Rev.* **2017**, DOI: 10.1128/MMBR.00048-16.

DOI: 10.1021/acscatal.9b00963
ACS Catal. 2019, 9, 6766−6782

(2) Dailey, H. A.; Gerdes, S.; Dailey, T. A.; Burch, J. S.; Phillips, J. D. Noncanonical Coproporphyrin-Dependent Bacterial Heme Biosynthesis Pathway That Does Not Use Protoporphyrin. *Proc. Natl. Acad. Sci. U. S. A.* **2015**, *112* (7), 2210−5.
(3) Hobbs, C.; Dailey, H. A.; Shepherd, M. The HemQ Coprohaem Decarboxylase Generates Reactive Oxygen Species: Implications for the Evolution of Classical Haem Biosynthesis. *Biochem. J.* **2016**, *473* (21), 3997−4009.
(4) Celis, A. I.; Streit, B. R.; Moraski, G. C.; Kant, R.; Lash, T. D.; Lukat-Rodgers, G. S.; Rodgers, K. R.; DuBois, J. L. Unusual Peroxide-Dependent, Heme-Transforming Reaction Catalyzed by HemQ. *Biochemistry* **2015**, *54* (26), 4022−32.
(5) Hofbauer, S.; Mlynek, G.; Milazzo, L.; Pühringer, D.; Maresch, D.; Schaffner, I.; Furtmüller, P. G.; Smulevich, G.; Djinovic-Carugo, K.; Obinger, C. Hydrogen Peroxide-Mediated Conversion of Coproheme to Heme b by HemQ-Lessons from the First Crystal Structure and Kinetic Studies. *FEBS J.* **2016**, *283* (23), 4386−4401.
(6) Celis, A. I.; Gauss, G. H.; Streit, B. R.; Shisler, K.; Moraski, G. C.; Rodgers, K. R.; Lukat-Rodgers, G. S.; Peters, J. W.; DuBois, J. L. Structure-Based Mechanism for Oxidative Decarboxylation Reactions Mediated by Amino Acids and Heme Propionates in Coproheme Decarboxylase (HemQ). *J. Am. Chem. Soc.* **2017**, *139* (5), 1900−1911.
(7) Streit, B. R.; Celis, A. I.; Shisler, K.; Rodgers, K. R.; Lukat-Rodgers, G. S.; DuBois, J. L. Reactions of Ferrous Coproheme Decarboxylase (HemQ) with O2 and H2O2 Yield Ferric Heme b. *Biochemistry* **2017**, *56* (1), 189−201.
(8) Hofbauer, S.; Dalla Sega, M.; Scheiblbrandner, S.; Jandova, Z.; Schaffner, I.; Mlynek, G.; Djinovic-Carugo, K.; Battistuzzi, G.; Furtmüller, P. G.; Oostenbrink, C.; Obinger, C. Chemistry and Molecular Dynamics Simulations of Heme b-HemQ and Coproheme-HemQ. *Biochemistry* **2016**, *55* (38), 5398−412.
(9) Hofbauer, S.; Hagmüller, A.; Schaffner, I.; Mlynek, G.; Krutzler, M.; Stadlmayr, G.; Pirker, K. F.; Obinger, C.; Daims, H.; Djinović-Carugo, K.; Furtmüller, P. G. Structure and Heme-Binding Properties of HemQ (Chlorite Dismutase-like Protein) from Listeria monocytogenes. *Arch. Biochem. Biophys.* **2015**, *574*, 36−48.
(10) Milazzo, L.; Hofbauer, S.; Howes, B. D.; Gabler, T.; Furtmüller, P. G.; Obinger, C.; Smulevich, G. Insights into the Active Site of Coproheme Decarboxylase from Listeria monocytogenes. *Biochemistry* **2018**, *57* (13), 2044−2057.
(11) Streit, B. R.; Celis, A. I.; Moraski, G. C.; Shisler, K. A.; Shepard, E. M.; Rodgers, K. R.; Lukat-Rodgers, G. S.; DuBois, J. L. Decarboxylation Involving a Ferryl, Propionate, and a Tyrosyl Group in a Radical Relay Yields Heme b. *J. Biol. Chem.* **2018**, *293* (11), 3989−3999.
(12) Pfanzagl, V.; Holcik, L.; Maresch, D.; Gorgone, G.; Michlits, H.; Furtmüller, P. G.; Hofbauer, S. Coproheme Decarboxylases - Phylogenetic Prediction versus Biochemical Experiments. *Arch. Biochem. Biophys.* **2018**, *640*, 27−36.
(13) Kostan, J.; Sjöblom, B.; Maixner, F.; Mlynek, G.; Furtmüller, P. G.; Obinger, C.; Wagner, M.; Daims, H.; Djinović-Carugo, K. Structural and Functional Characterisation of the Chlorite Dismutase from the Nitrite-oxidizing Bacterium "Candidatus Nitrospira defluvii": Identification of a Catalytically Important Amino Acid Residue. *J. Struct. Biol.* **2010**, *172* (3), 331−42.
(14) Goblirsch, B. R.; Streit, B. R.; Dubois, J. L.; Wilmot, C. M. Structural Features Promoting Dioxygen Production by Dechloromonas aromatica Chlorite Dismutase. *JBIC, J. Biol. Inorg. Chem.* **2010**, *15* (6), 879−88.
(15) Dijkstra, E. A Note on Two Problems in Connexion with Graphs. *Numerische Mathematik* **1959**, *1* (1), 269−271.
(16) Beratan, D.; Onuchic, J.; Betts, J.; Bowler, B.; Gray, H. Eelectron-Tunneling Pathwaysin Ruthenated Proteins. *J. Am. Chem. Soc.* **1990**, *112* (22), 7915−7921.
(17) Sündermann, A.; Oostenbrink, C. Molecular Dynamics Simulations Give Insight into the Conformational Change, Complex Formation, and Electron Transfer Pathway for Cytochrome P450 Reductase. *Protein Sci.* **2013**, *22* (9), 1183−95.
(18) Milazzo, L.; Gabler, T.; Pfanzagl, V.; Michlits, H.; Furtmüller, P. G.; Obinger, C.; Hofbauer, S.; Smulevich, G. The Hydrogen Bonding Network of Coproheme in Coproheme Decarboxylase from Listeria monocytogenes: Effect on Structure and Catalysis. *J. Inorg. Biochem.* **2019**, *195*, 61−70.
(19) Jakopitsch, C.; Spalteholz, H.; Furtmüller, P. G.; Arnhold, J.; Obinger, C. Mechanism of Reaction of Horseradish Peroxidase with Chlorite and Chlorine Dioxide. *J. Inorg. Biochem.* **2008**, *102* (2), 293−302.
(20) Jakopitsch, C.; Pirker, K. F.; Flemmig, J.; Hofbauer, S.; Schlorke, D.; Furtmüller, P. G.; Arnhold, J.; Obinger, C. Mechanism of Reaction of Chlorite with Mammalian Heme Peroxidases. *J. Inorg. Biochem.* **2014**, *135*, 10−9.
(21) Obinger, C. A Protein Fold with Multiple Functions: Chlorite Dismutase, HemQ and DyP-type Peroxidase. *Arch. Biochem. Biophys.* **2015**, *574*, 1−2.
(22) Chen, Y. R.; Chen, C. L.; Chen, W.; Zweier, J. L.; Augusto, O.; Radi, R.; Mason, R. P. Formation of Protein Tyrosine Ortho-Semiquinone Radical and Nitrotyrosine from Cytochrome c-Derived Tyrosyl Radical. *J. Biol. Chem.* **2004**, *279* (17), 18054−62.
(23) Cerda-Colon, J.; Silfa, E.; Lopez-Garriga, J. Unusual Rocking Freedom of the Heme in the Hydrogen Sulfide-Binding Hemoglobin from Lucina pectinata. *J. Am. Chem. Soc.* **1998**, *120* (36), 9312−9317.
(24) Smulevich, G.; Mantini, A. R.; English, A. M.; Mauro, J. M. Effects of Temperature and Glycerol on the Resonance Raman Spectra of Cytochrome c Peroxidase and Selected Mutants. *Biochemistry* **1989**, *28* (12), 5058−64.
(25) Smulevich, G.; Wang, Y.; Edwards, S. L.; Poulos, T. L.; English, A. M.; Spiro, T. G. Resonance Raman Spectroscopy of Cytochrome c Peroxidase Single Crystals on a Variable-Temperature Microscope Stage. *Biochemistry* **1990**, *29* (10), 2586−92.
(26) Howes, B. D.; Feis, A.; Indiani, C.; Marzocchi, M. P.; Smulevich, G. Formation of Two Types of Low-Spin Heme in Horseradish Peroxidase Isoenzyme A2 at Low Temperature. *JBIC, J. Biol. Inorg. Chem.* **2000**, *5* (2), 227−35.
(27) Nielsen, K. L.; Indiani, C.; Henriksen, A.; Feis, A.; Becucci, M.; Gajhede, M.; Smulevich, G.; Welinder, K. G. Differential Activity and Structure of Highly Similar Peroxidases. Spectroscopic, Crystallographic, and Enzymatic Analyses of Lignifying Arabidopsis thaliana Peroxidase A2 and Horseradish Peroxidase A2. *Biochemistry* **2001**, *40* (37), 11013−21.
(28) Marzocchi, M.; Smulevich, G. Relationship Between Heme Vinyl Conformation and the Protein Matrix in Peroxidases. *J. Raman Spectrosc.* **2003**, *34* (10), 725−736.
(29) Smulevich, G.; Hu, S.; Rodgers, K.; Goodin, D.; Smith, K.; Spiro, T. Heme-Protein Interactions in Cytochrome c Peroxidase Revealed by Site-Directed Mutagenesis and Resonance Raman Spectra of Isotopically Labeled Hemes. *Biospectroscopy* **1996**, *2* (6), 365−376.
(30) Nagradova, N. Interdomain Communications in Bifunctional Enzymes: How are Different Activities Coordinated? *IUBMB Life* **2003**, *55* (8), 459−66.
(31) Wacker, H.; Aggeler, R.; Kretchmer, N.; O'Neill, B.; Takesue, Y.; Semenza, G. A Two-Active Site One-Polypeptide Enzyme: the Isomaltase From Sea Lion Small Intestinal Brush-Border Membrane. Its Possible Phylogenetic Relationship with Sucrase-Isomaltase. *J. Biol. Chem.* **1984**, *259* (8), 4878−84.
(32) LaPorte, D. C.; Koshland, D. E. A Protein with Kinase and Phosphatase Activities Involved in Regulation of Tricarboxylic Acid Cycle. *Nature* **1982**, *300* (5891), 458−60.
(33) Graf, M. M.; Sucharitakul, J.; Bren, U.; Chu, D. B.; Koellensperger, G.; Hann, S.; Furtmüller, P. G.; Obinger, C.; Peterbauer, C. K.; Oostenbrink, C.; Chaiyen, P.; Haltrich, D. Reaction of Pyranose Dehydrogenase from Agaricus meleagris with Its Carbohydrate Substrates. *FEBS J.* **2015**, *282* (21), 4218−41.
(34) Wongnate, T.; Sucharitakul, J.; Chaiyen, P. Identification of a Catalytic Base for Sugar Oxidation in the Pyranose 2-Oxidase Reaction. *ChemBioChem* **2011**, *12* (17), 2577−86.

DOI: 10.1021/acscatal.9b00963
ACS Catal. 2019, 9, 6766−6782

(35) Hernández-Ortega, A.; Lucas, F.; Ferreira, P.; Medina, M.; Guallar, V.; Martínez, A. T. Role of Active Site Histidines in the Two Half-Reactions of the Aryl-Alcohol Oxidase Catalytic Cycle. *Biochemistry* **2012**, *51* (33), 6595−608.
(36) Mercadante, D.; Melton, L. D.; Jameson, G. B.; Williams, M. A.; De Simone, A. Substrate Dynamics in Enzyme Action: Rotations of Monosaccharide Subunits in the Binding Groove are Essential for Pectin Methylesterase Processivity. *Biophys. J.* **2013**, *104* (8), 1731−9.
(37) Lobo, S. A.; Scott, A.; Videira, M. A.; Winpenny, D.; Gardner, M.; Palmer, M. J.; Schroeder, S.; Lawrence, A. D.; Parkinson, T.; Warren, M. J.; Saraiva, L. M. Staphylococcus aureus Haem Biosynthesis: Characterisation of the Enzymes Involved in Final Steps of the Pathway. *Mol. Microbiol.* **2015**, *97* (3), 472−87.

NOTE ADDED AFTER ASAP PUBLICATION

This paper was published on the Web on July 1, 2019, with minor errors in the text and an error in Table 4. The corrected version was reposted on July 3, 2019.

DOI: 10.1021/acscatal.9b00963
ACS Catal. 2019, 9, 6766−6782